Measurement report: Observation-based formaldehyde production rates and their relation to OH reactivity around the Arabian Peninsula

Dirk Dienhart[1], John N. Crowley[1], Efstratios Bourtsoukidis[2], Achim Edtbauer[1], Philipp G. Eger[1], Lisa Ernle[1], Hartwig Harder[1], Bettina Hottmann[1], Monica Martinez[1], Uwe Parchatka[1], Jean-Daniel Paris[3,2], Eva Y. Pfannerstill[1], Roland Rohloff[1], Jan Schuladen[1], Christof Stönner[1], Ivan Tadic[1], Sebastian Tauer[1], Nijing Wang[1], Jonathan Williams[1,2], Jos Lelieveld[1,2] and Horst Fischer[1]

[1]Atmospheric Chemistry Department, Max Planck Institute for Chemistry, Mainz, Germany
[2] Climate and Atmosphere Research Centre, The Cyprus Institute, Nicosia, Cyprus
[3] Laboratoire des Sciences du Climat et de l'Environnement, CEA-CNRS-UVSQ, UMR8212, IPSL, Gif-sur-Yvette, France

Correspondence to: Dirk Dienhart (D.Dienhart@mpic.de) or Horst Fischer (Horst.Fischer@mpic.de)

Abstract. Formaldehyde (HCHO) is the most abundant aldehyde in the troposphere. While its background-mixing ratio is mostly determined by the oxidation of methane, in many environments, especially in the boundary layer, HCHO can have a large variety of precursors, in particular biogenic and anthropogenic volatile organic compounds (VOCs) and their oxidation products. Here we present shipborne observations of HCHO, hydroxyl radical (OH) and OH reactivity (R(OH)), obtained during the Air Quality and Climate Change in the Arabian Basin (AQABA) campaign in summer 2017. The loss rate of HCHO was inferred from its reaction with OH, measured photolysis rates, and dry deposition. In photo-stationary state, the HCHO loss is balanced by production via OH initiated degradation of volatile organic compounds (VOCs), photolysis of oxygenated volatile organic compounds (OVOCs) and the ozonolysis of alkenes. The slope α from a scatter plot of the HCHO production rate versus the product of R(OH) and OH yields the fraction of R(OH) that contributes to HCHO production. Values of α varied between less than 2 % in rather clean air over the Arabian Sea and the southern Red Sea, and up to 32 % over the polluted Arabian Gulf (also known as the Persian Gulf), signifying that polluted areas harbour a larger variety of HCHO precursors. The HCHO yield from R(OH) depends on the absolute and relative contributions of alkanes, alkenes, oxygenated volatile organic compounds (OVOCs) and aromatics to R(OH), while no significant correlation to NO_x mixing ratios was found, indicating that HCHO production was not NO_x limited.

1 Introduction

Formaldehyde (HCHO) is a ubiquitous trace gas, which is highly reactive and provides a source of hydroperoxyl radicals (HO_2) via its photolysis. HCHO can be emitted directly from a variety of both biogenic (including biomass burning) and anthropogenic sources, but is also a by-product of the oxidation of several volatile organic compounds (VOCs) and their photolysis (Stickler et al., 2006; Anderson et al., 2017). It is the most abundant aldehyde in the atmosphere and one of the few

oxygenated volatile organic compounds (OVOCs) that can be measured directly from satellites (De Smedt et al., 2008; Marbach et al., 2009; De Smedt et al., 2012; De Smedt et al., 2015; De Smedt et al., 2018, Zhu et al., 2020). In particular, the ability to measure HCHO from satellites has instigated several studies on the relation between HCHO column densities and emissions of isoprene, one of its dominant biogenic precursors (Palmer et al., 2003; Shim et al., 2005; Millet et al., 2008;

5   Wolfe et al., 2016). In most of the free troposphere and the remote marine boundary layer, HCHO mixing ratios are determined by methane (CH_4) oxidation (Ayers et al., 1997; Weller et al., 2000; Wagner et al., 2002) and degradation of the oxidation products methanol (CH_3OH), methylhydroperoxide (CH_3OOH), and of other ubiquitous OVOCs like acetone (Kormann et al., 2003; Reeves and Penkett 2003; Stickler et al., 2006; Anderson et al., 2017). In polluted areas, the oxidation of a large variety of biogenic and anthropogenic precursors contributes to HCHO production (Liu et al., 2007; DiGangi et al., 2012; Wolfe et

10 al., 2016, Wennberg et al., 2018, Kluge et al., 2020). HCHO/NO_2 ratios have been frequently used to differentiate between nitrogen oxide ($NO_x = NO + NO_2$) and VOC limited ozone production (Martin et al., 2004; Duncan et al., 2010; Schroeder et al., 2017; Tadic et al., 2020) and to infer global hydroxyl radical (OH) concentrations (Wolfe et al., 2019). If HCHO loss rates are well defined, estimation of the concentrations of OH from HCHO mixing ratios is feasible since HCHO production is dominated by the oxidation of VOCs via OH.

15 Formaldehyde production in the troposphere results from reactions of VOCs with OH, ozone (O_3) and the nitrate radical (NO_3), with the oxidation processes to be dominated by OH over the day, and by NO_3 during night, for many trace-gases of biogenic origin. Liebmann et al. (2018) showed that the daytime loss of biogenic compounds via reaction with NO_3 can also be significant in forested areas. Unsaturated hydrocarbons (e.g. ethene, isoprene and terpenes) additionally react with O_3 in the form of a cycloaddition to form energy-rich primary ozonides (Criegee intermediates) that rapidly fragment, releasing HCHO

20 (Cox et al., 2020). This class of reactions is most important in relation to biogenic emissions in forested regions. Many OVOCs (e.g. alcohols, aldehydes, hydroperoxides, or alkylnitrates) also produce HCHO in reactions with OH, chlorine radicals or via photolysis. Alkanes react with OH forming saturated peroxy radicals (RO_2) that further react with NO to form alkoxy radicals and subsequently carbonyl compounds including HCHO. Since the oxidation of almost every VOC can produce HCHO, some with a yield greater than unity (Luecken et al., 2018), HCHO is an ideal candidate to test our understanding of VOC chemistry

25 using zero dimensional box (Wagner et al., 2002; Fried et al., 2011) and three dimensional general circulation models (Kormann et al., 2003; Liu et al. 2007; Klippel et al., 2011; Anderson et al., 2017; Dienhart et al. 2021).

In addition to summing up the contributions of individual HCHO production pathways, the production rate of HCHO resulting from reactions involving OH chemistry ($P_{OH}(HCHO)$) can be deduced from the OH concentration ([OH]), the yield α and the OH reactivity (R(OH)) which is a summation of all reactions with trace gas R_i that react with OH and the rate coefficient k_i

30 (Liu et al. 2017; Wolfe et al., 2019):

$$P_{OH}(HCHO) = \alpha \cdot [OH] \cdot R(OH) \qquad\qquad (1)$$

with

$$R(OH) = \sum k_i \cdot R_i \qquad\qquad (2)$$

R(OH) thus includes reactions of OH with species like e.g. carbon monoxide (CO), sulphur dioxide (SO_2), nitrogen dioxide (NO_2) or nitric acid (HNO_3) that do not result in HCHO formation as well as reaction with VOCs like methane, alkanes, alkenes, aromatics or OVOCs (Williams and Brune, 2015). Calculating P_{OH}(HCHO) this way has the advantage that reactions of non-measured VOCs with OH will be included. Not all reactions with OH will produce HCHO, which is accounted for by the yield factor α (Wolfe et al., 2019), which is a summation over the HCHO yield α_i of each $k_i \times R_i$. For reactants that yield no HCHO (e.g. CO, NO_2, SO_2, HNO_3 and HCHO itself), α_i is zero. Species that yield HCHO have positive α_i values (e.g. CH_4, isoprene, etc.). Note that the individual α_i and thus the overall α can be functions of NO_x (Wolfe et al., 2016). For example, the yield of HCHO from methane oxidation depends on the fate of the initially formed methyl peroxy radical (CH_3O_2). At high NO_x levels, CH_3O_2 will react with NO, subsequently forming HCHO. At low NO_x, CH_3O_2 preferentially reacts with the hydroperoxy radical (HO_2) forming methyl hydroperoxide (CH_3OOH), reducing the immediate yield of HCHO production from CH_4 oxidation (Wagner et al., 2002). To calculate the total production rate P(HCHO), additional direct emissions of HCHO or its production due to photolysis (e.g. CH_3OOH, acetaldehyde (CH_3CHO) and further OVOCs) and the ozonolysis of alkenes (Stickler et al., 2006; Parrish et al., 2012; Anderson et al., 2017) have to be included as P_{add}(HCHO):

$$P(HCHO) = P_{OH}(HCHO) + P_{add}(HCHO) \tag{3}$$

In photo-stationary state (PSS), P(HCHO) is expected to be balanced by HCHO losses (L(HCHO)). PSS is most likely to be achieved at midday ($j_{HCHO} \sim 7 \times 10^{-5}$; R(OH + HCHO) $\sim 4 \times 10^{-5}$) when the formaldehyde lifetime is ~ 2.5 hours.

$$P(HCHO) = L(HCHO) = \left(k_{OH+HCHO} \cdot [OH] + j_{HCHO} + \frac{v_d}{BLH} \right) \cdot [HCHO] \tag{4}$$

The first term within brackets in Eq. 4 represents HCHO loss due to reaction with OH radicals, while the second term describes total losses due to photolysis (both the radical and molecular channel). In the boundary layer, additional loss due to dry deposition has to be considered, and depends on the deposition velocity v_d and the boundary layer height (BLH). Further loss due to rain-out has been neglected in this study since we did not encounter significant precipitation during the AQABA campaign.

In this analysis we use in situ observations of HCHO, OH, R(OH) and j_{HCHO} together with the HCHO deposition velocity v_d (calculated for 34 m above the ocean, Stickler et al., 2007) and ERA-5 meteorological data of the BLH (https://www.ecmwf.int/en/forecasts/datasets/reanalysis-datasets/era5), obtained during a ship-cruise around the Arabian Peninsula as part of the AQABA (Air Quality and Climate in the Arabian Basin) campaign in summer 2017. From this dataset, we calculated the production and loss rates of HCHO. Scatter plots of [OH] $\times$ R(OH) versus P(HCHO) yielded values for the

formaldehyde yield α in different geographical regions, reflecting the transition between rather clean to highly polluted conditions, both with respect to NO_x and VOCs.

$$\alpha = \frac{P(HCHO) - P_0(HCHO)}{[OH] \cdot R(OH)} \qquad (5)$$

5

The major questions addressed in this study are:

1. Are reactions involving OH the dominant HCHO source in different regions around the Arabian Peninsula, or do photolysis (e.g. of oxidised organics), reactions (e.g. of unsaturated hydrocarbons) with O_3 or direct emission significantly contribute to HCHO formation?

10 2. What is the contribution of different VOC compound classes (alkanes, alkenes, aromatics, OVOC) to α in Eq. 1?

3. Does α depend on NO_x?

In section 2, we give a brief outline of the AQABA cruise and the measurements performed. An investigation of the balance between HCHO production via the product of R(OH) and OH (Eq. 1) and production deduced from HCHO loss assuming PSS (Eq. 3) is given in section 3. Section 4 covers a discussion of the variation of α in different regions, a summary of the results

15 obtained is presented in section 5.

2 Measurements during AQABA

Measurements during AQABA took place on board the research and survey vessel *Kommandor Iona* from 25 June to 3 September 2017. The first leg from southern France to Kuwait started in La-Seyne-sur-Mer (near Toulon, France) and continued via the Mediterranean, the Suez Canal, the Red Sea, the Arabian Sea, the Gulf of Oman and the Arabian Gulf (also
5 known as the Persian Gulf) to Kuwait. During the second leg, the vessel returned via the same route (Fig. 1).

Four laboratory containers with instrumentation for in situ and offline monitoring of a large suite of trace gases, particles and radicals were mounted on the front deck of the ship. With the exception of aerosols and radical measurements (OH and HO_2), air sampling was achieved from a high-flow ($10 \; m^3 \; min^{-1}$) cylindrical stainless steel inlet (HFI, sampling height: 5.5 m above deck, diameter: 0.2 m), placed between the containers on the front deck of the ship. Air was drawn from the center of the HFI
10 into the air-conditioned laboratory containers using PFA (perfluoroalkoxy alkane) tubing. The inlet for OH and HO_2 measurements was mounted on top of a laboratory container closest to the bow.

Formaldehyde measurements were based on the Hantzsch technique using a commercial instrument (Aero-Laser, model AL4021, Garmisch-Partenkirchen, Germany). The limit of detection (LOD), determined from the reproducibility of on-board zero air measurements was between 80 and 128 pptv (influenced by wave-induced rolling of the ship) with a confidence
15 interval of 1σ. The total measurement uncertainty including line losses was 13 % (Dienhart et al., 2021).

Measurements of OH radicals were performed using laser induced fluorescence with the HORUS instrument based on laser induced fluorescence detection (Martinez et al., 2010; Hens et al., 2014, Marno et al., 2020). Typical detection limits for OH were between 1×10^5 and 5×10^5 molec cm^{-3} with the total uncertainty of ~ 30 %. OH measurements below the instrumental LOD were excluded from this study. Note that an inlet pre-injector (IPI) was used to determine the OH background signal via
20 chemical modulation (Novelli et al., 2014).

Total OH reactivity was measured using the comparative reactivity method (Sinha et al., 2008, Fuchs et al., 2017). A detailed description of the measurement technique and the results from the AQABA campaign can be found in Pfannerstill et al. (2019). The 5 min detection limit was 5.4 s^{-1}, derived from the 2σ standard deviation of clean air measurements over the Arabian Sea. Total uncertainty (1σ) of the OH reactivity measurements was 7–60 %.

25 Nitrogen oxides ($NO_x = NO + NO_2$) were measured with a two-channel chemiluminescence instrument CLD 790 SR (ECO Physics AG, Dürnten, Switzerland). A detailed description of the instrument during AQABA can be found in Tadic et al. (2020). The measurement uncertainty of the NO data was calculated to be 6 % at 5 min integration time and a confidence level of 1σ. The LOD for the NO channel was estimated as the full width at half maximum of the frequency distribution of all zero air measurements obtained during the campaign to be 9 pptv with a confidence level of 1σ. The total uncertainty of the NO_2
30 data was estimated as a conservative upper limit at 23 % as the average of the relative uncertainties of all data points obtained during the campaign. The absolute detection limit of the NO_2 instrument was estimated at 112 pptv (Tadic et al. 2020).

O₃ measurements were performed with a commercial absorption photometer (Model 202 Ozone Monitor, 2B Technologies, Boulder, Colorado). Water and particle interferences during the expedition were minimized by sampling through a Nafion tube and a Teflon filter, the overall uncertainty of the data was 2 % (Tadic et al. 2020).

CO mixing ratios were determined with a cavity ring-down spectrometer (Picarro G2401; Santa Clara, USA) with a precision

5 of ≤ 8 ppbv. The CO mixing ratio was further corrected for water vapor effects and has been quality-controlled following ICOS (Integrated Carbon Observing System) standards, further details can be found in Paris et al. (2021).

Sulfur dioxide (SO_2) was detected with a chemical ionization quadrupole mass spectrometer (CI-QMS) using an electrical, radio-frequency discharge ion source with a detection limit of 38 pptv and a total uncertainty of 20 % ± 23 pptv. Further details about the instrument and ionization method are described in Eger et al. (2019).

10 Photolysis rates for a large number of trace gases were calculated from wavelength resolved actinic flux measurements with a spectral radiometer (Metcon GmbH, Glashütten, Germany) located approximately 10 m above sea level (~ 5 m above the front deck). The total uncertainty of the HCHO photolysis rates obtained are ~ 10 %, based on the calibration of the instrument (Bohn et al., 2008) and the data was not corrected for upwelling radiation, which is considered to be insignificant at the sea surface.

15 As the sampling location was in front of the ship's chimney, contamination of the measurements with the ship's own exhaust occurred when the vessel was sailing ahead of the wind. Thus, a data-filter based on relative wind direction and NO, CO and SO_2 observations was used to eliminate contaminated data (including other ship exhausts and the stop in Jeddah and Kuwait). This affected mainly the measurements during the first leg of the cruise (Tadic et al., 2020).
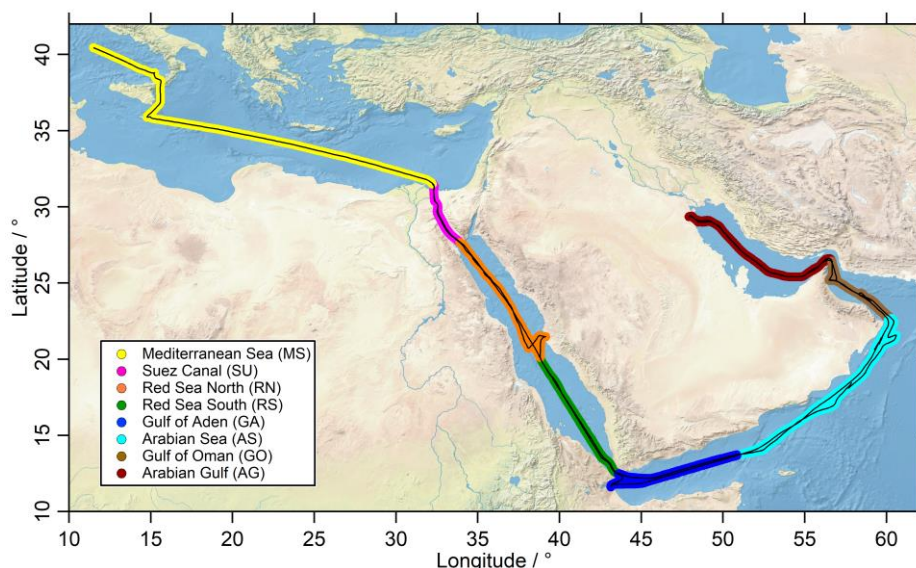
20 **Figure 1**: The shiptrack (black) of the Kommandor Iona during the AQABA cruise subdivided into eight regions: Mediterranean sea (MS: yellow), Suez Canal (SU: pink), Read Sea North (RN: orange), Read Sea South (RS: green), Gulf of Aden (GA: blue), Arabian Sea (AS: turquoise), Gulf of Oman (GO: brown) and Arabian Gulf (AG: red).

Atmospheric
Chemistry
and Physics
Discussions

3 Results

The daytime observations of HCHO, OH, R(OH) and the photolysis rate of HCHO (j_{HCHO}) during the AQABA cruise are displayed in Fig. 2. Note that only observations after 20 July 2017 (the start of the OH measurements) were used in this study. Formaldehyde mixing ratios varied between minimum values of approximately 0.1 ppbv over the Arabian Sea during the first

5   leg (AS Leg 1; 20–23 July) and the Red Sea South (RS; 17–19 August) up to more than 10 ppbv over the Arabian Gulf (AG; 28 July to 5 August). The highest values were detected at the center of the Gulf, coincident with the highest ozone (O_3) mixing ratios > 150 ppbv during AQABA (Tadic et al., 2020). Simultaneously, elevated ethene (Bourtsoukidis et al., 2019), OVOCs (Wang et al., 2020) and organic peroxides (Dienhart et al., 2021) highlight this area as a hotspot of air pollution. Median HCHO concentrations between 1 and 2 ppbv were measured in most of the other regions (Mediterranean Sea (MS); Red Sea

10 North (RN); Gulf of Aden (GA), Arabian Sea Leg 2 (AS Leg 2); Gulf of Oman (OG)), while pollution events also occurred in the area around the Suez Canal (SU). In general, diurnal variations of HCHO with maximum values around local noon were observed on most days.

Strong diurnal variations were observed for OH mixing ratios with noontime maximum values varying between 0.1 and 0.5 pptv in most regions. The highest noontime mixing ratios (~ 0.8 pptv) were observed over the Gulf of Aden (GA;

15 16 August). Although there is some regional variation, there is no clear trend with respect to the different locations, as for example found for HCHO mixing ratios.

Large regional variations were also found for the OH reactivity, with noontime values ranging from close to the detection limit in the Arabian Sea (AS leg 1 and 2), the Gulf of Aden (GA) and the Red Sea (RS and RN) to values of more than 30 s^{-1}, predominately in the polluted regions of the Arabian Gulf (AG) and the Suez Canal (SU). For a detailed discussion of the OH

20 reactivity in different regions and its relations to VOCs and inorganic compounds see Pfannerstill et al. (2019).

Noontime-maxima in the formaldehyde photolysis rates varied between 45×10^{-6} and 78×10^{-6} s^{-1}. On most days, clear diurnal profiles were observed under clear sky conditions. Significant cloud cover was observed only on 20–22 July and 08–10 August. The boundary layer height varied between 250–1400 m (Fig. 2), with least diurnal variation in the Arabian and the Mediterranean Sea with a mean of 566 m and 780 m, respectively. The boundary layer height in other regions was more

25 variable, with a mean value for the entire dataset (excluding the stop in Kuwait) of 750 m.
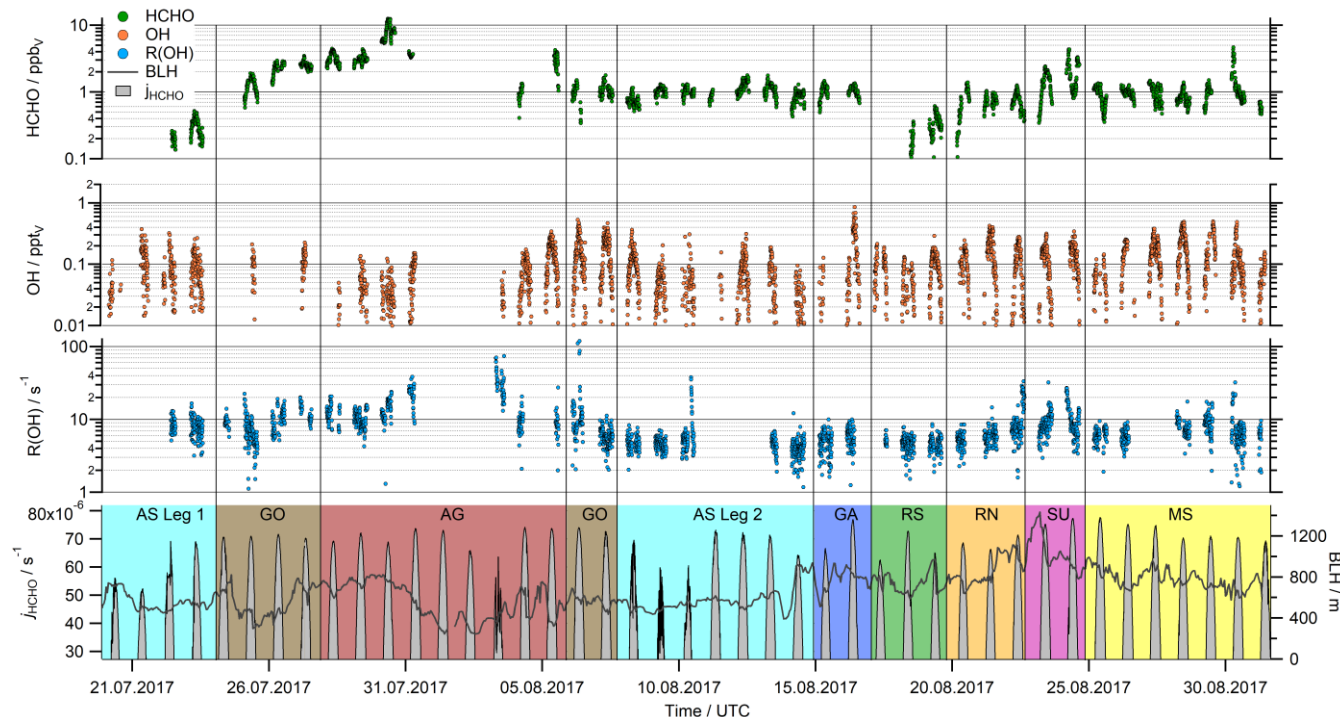
Figure 2: Time series of HCHO, OH, R(OH) and the HCHO photolysis (j_{HCHO}, sum of the molecular and the radical channel) in 5 min resolution. For the boundary layer height (BLH) we used the ERA-5 meteorological reanalysis data in hourly averages, which resolves the earth's atmosphere on a 30 km grid (https://www.ecmwf.int/en/forecasts/datasets/reanalysis-datasets/era5).

5

The sink of HCHO was calculated by summing the loss rate coefficients through reaction with OH, photolysis and dry deposition (Eq. 4, Fig. 3). Based on Gaussian error propagation of uncertainty in the HCHO and OH mixing ratios, j_{HCHO}, and the rate coefficient k_{OH} for reaction of OH with HCHO, the total uncertainties of the loss rates due to OH and j_{HCHO} are 33 % and 15 %, respectively. Loss of HCHO via photolysis and reaction with OH were found to be of the same order of magnitude,

10 with total, noontime loss rates varying from 0.01 pptv s^{-1} up to 1 pptv s^{-1}. The formaldehyde sinks due to OH and photolysis were of the order of 0.1 pptv s^{-1} during noon, with the lowest values over the Arabian Sea, the Gulf of Aden (08–15 August) and the southern Red Sea (18–20 August). Significantly enhanced noontime values (> 0.2 pptv s^{-1}) were found for the loss through photolysis in the Arabian Gulf (28–31 August) due to the elevated HCHO mixing ratios.

The removal of HCHO by dry deposition depends on turbulent transport and also on the wind speed. Since our results for the

15 HCHO mixing ratio are just one dimensional, the dry deposition could not be calculated directly for the AQABA dataset and was thus inferred with the literature value for the HCHO deposition velocity (v_d) over sea and the boundary layer height. In our analysis we used a fixed value of 0.36 ± 0.11 cm s^{-1} for v_d based on the findings of Stickler et al. (2007). For the BLH we used the mean value of the ERA-5 results (750 ± 113 m) instead of the values shown in Fig. 2, since the highest available resolution was 30 minutes. Performing the analysis with the lower time resolution resulted in less data coverage for the scatter

plots and thus we decided to use the mean value instead. Assuming an uncertainty of 30 % for v_d and 15 % for the BLH as conservative estimate, results in an uncertainty of 34 % for the dry deposition term.

Close to local noon, the loss rate due to dry deposition was in general below 0.1 pptv s^{-1} and thus much smaller than HCHO removal by either photolysis or reaction with OH (Fig. 3). Only close to sunrise and sunset dry deposition was of similar
5   magnitude to photochemical loss processes. The lowest panel in Fig. 3 shows the sum of all three loss processes according to Eq. 4. Based on Gaussian error propagation the estimated uncertainty of L(HCHO) is 52 %.
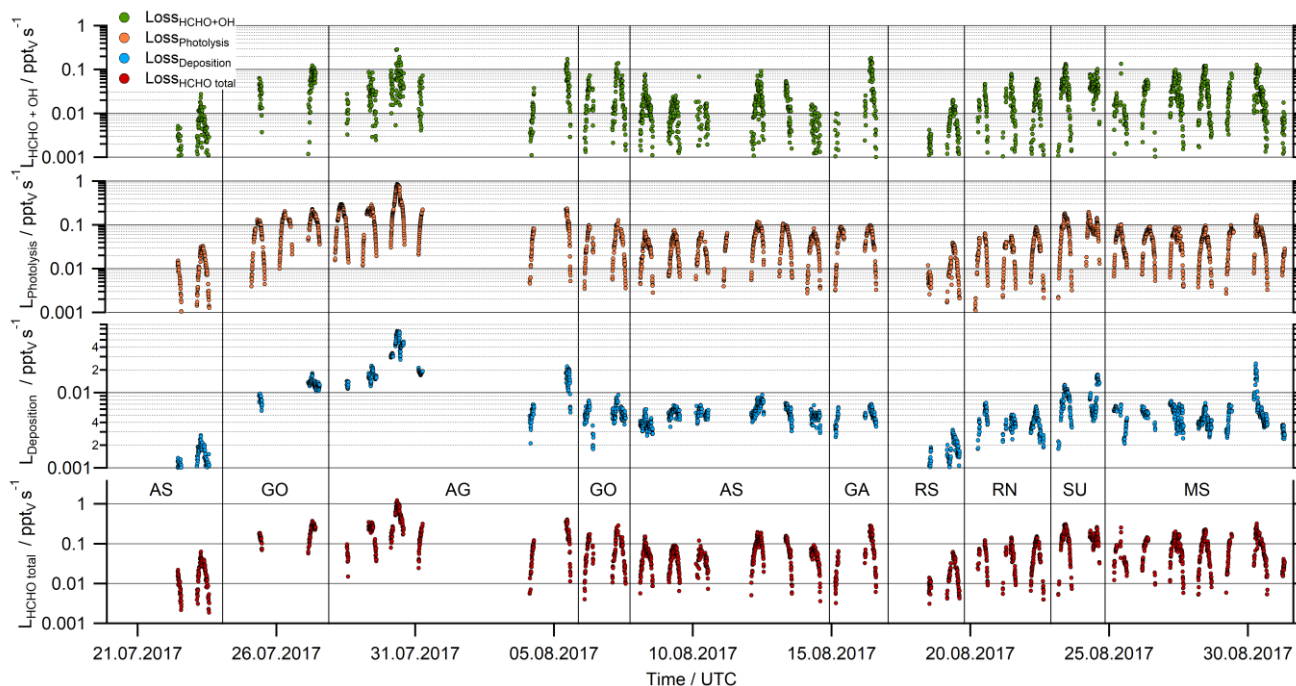
Figure 3: HCHO loss rates due to reaction with OH, photolysis, dry deposition and the total sink as the sum of all three processes.

10

In photo-stationary state the HCHO loss and production balance, and a scatter plot of the product of the OH reactivity R(OH) (s^{-1}) and the OH mixing ratio (pptv) versus the HCHO production rate P(HCHO) (=L$_{HCHO\ total}$) yields the slope, i.e. the factor α according to Eq. 5 (Fig. 4). A compact linear relationship is expected under PSS conditions (HCHO lifetime ~ 2.5 h), while data points that do not fulfill PSS, e.g. due to sporadic direct emissions from point sources, or advection of HCHO enriched or
15   depleted air masses are expected not to follow the regression line, yielding low R^2 values. For example, a fresh pollution plume (e.g. containing unsaturated hydrocarbons) will result in data shifted below the regression line since a high OH reactivity is expected along with low HCHO production, as secondary processes taking place over longer time-scales (e.g. photolysis) are involved in the HCHO production from unsaturated hydrocarbons. Rainout would also result in data points below the regression, while primary emission from point sources will shift data above the regression line due to the correlation with the
20   HCHO mixing ratio. Non-zero P(HCHO) at zero [OH] × R(OH) corresponding to the intercept of the linear regression

indicates HCHO production by other sources than OH oxidation and represents P_{add}(HCHO) in Eq. 5. Thus it is an indication for additional HCHO sources due to direct emissions, photolysis of HCHO precursors or reactions of alkenes with O_3.

In our analysis, we first subdivided the data into the smaller regions according to Fig. 1 and examined the correlation between P(HCHO) and $[OH] \times R(OH)$ for each sub-region (Fig. 4). For the Arabian Sea, the dataset has been further partitioned into

5   the two individual legs heading towards and away from the Gulf of Oman. This is justified by the significant differences in HCHO mixing ratios and R(OH) during the two legs (AS Leg 1 and AS Leg 2) reflecting different air-mass origins. For the individual regions bivariate fits were performed according to York et al. (2004). In general, values of R^2 varied between 0.08 (Arabian Gulf) to 0.82 for the Gulf of Aden, while the slopes (α) varied between less than 0.02 for the Arabian Sea during the first leg and the southern Red Sea up to 0.26 for the Arabian Gulf. The values of α thus derived are lower limits, as R(OH)

10   includes reactions with inorganic trace-gases and others that do not yield HCHO (e.g. CO, NO_2 and SO_2). In general, the inorganics and CO account for ~ 10 % of the reactivity, except for the Suez Canal (~ 16 %) (see Table 1 in Pfannerstill et al., 2019). Values for the intercept b (P_{add}(HCHO)) were less or equal to 0.05 pptv s^{-1} in most regions, the cleanest regions with respect to NO_x and VOCs showed very low values for P_{add}(HCHO) with approximately 0.01 pptv s^{-1} over the Arabian Sea during the first leg and the southern Red Sea, indicating that HCHO production was dominated by OH chemistry. Highest

15   values of P_{add}(HCHO) were found over the Arabian Gulf (0.14 pptv s^{-1}) and the area around the Suez Canal (0.09 pptv s^{-1}), where enhanced mixing ratios of unsaturated hydrocarbons and OVOCs (Wang et al., 2020) as well as elevated O_3 mixing ratios prevailed (Tadic et al., 2020).

The same analysis was performed with the effective OH reactivity ($R(OH)_{eff}$) for which the contribution of NO_x, CO, SO_2, O_3 and HCHO has been removed (Fig. S1). The highest contribution by inorganic trace-gases to R(OH) was found over the

20   Arabian Gulf, the Gulf of Oman and while passing the street of Messina. Over the Arabian Gulf the correction was dominated by contributions from CO, O_3 and HCHO; while elevated NO_x mixing ratios contributed significantly over the Gulf of Oman and while passing the street of Messina (30.08.2017). Use of $R(OH)_{eff}$ resulted in a smaller data set and an increased slope (Fig. S2) compared to when using non-adjusted R(OH) and thus a higher yield α_{eff} for five sub-regions (Suez, Arabian Gulf, Gulf of Oman, Gulf of Aden, Arabian Sea Leg 2). No significant difference on α when using R(OH) and $R(OH)_{eff}$ was observed

25   for the remaining sub-regions, while the scatter plots show in general slightly reduced scatter and less data coverage. Values for the intercept b (P_{add}(HCHO)) were not significantly affected by choice of R(OH) or $R(OH)_{eff}$ and both methods yielded very similar results within their uncertainties, except for the Arabian Sea during the second leg, where P_{add}(HCHO) decreased to similar values of the Mediterranean Sea when $R(OH)_{eff}$ was used.

Atmospheric
Chemistry
and Physics
Discussions
Open Access
EGU
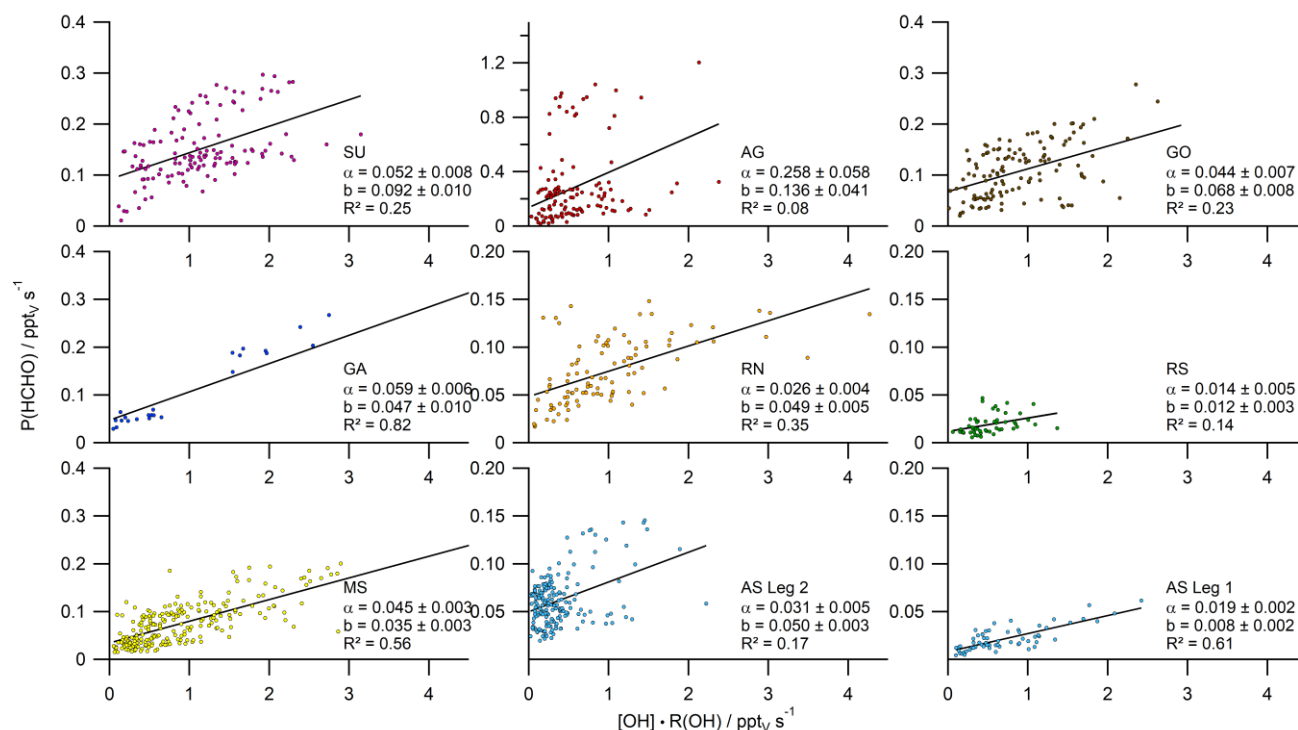
Figure 4: Scatter plots with bivariate fits (York et al., 2004) of the product [OH] × R(OH) versus the HCHO production rate, subdivided into the different regions probed during the AQABA cruise. The HCHO yield α is the slope of the respective regression, while the intercept represents additional HCHO sources not related to OH chemistry (P_{add}(HCHO)).

4 Discussion

The values of [OH] × R(OH) vary between practically zero and more than 4 pptv s^{-1} with maximum values over the northern Red Sea, the Mediterranean and the Gulf of Aden, while most data represents values ≥ 3 pptv s^{-1}. According to Eq. 4, formaldehyde loss L(HCHO) is the product of the HCHO mixing ratio and the loss rates due to reaction with OH, photolysis and dry deposition. In photo-stationary state (lifetime of HCHO ~ 2.5 h), formaldehyde loss is equal to its production P(HCHO) (Eq. 4). P(HCHO) varied between 0 and approximately 1.2 pptv s^{-1}, with the highest values above 0.4 pptv s^{-1} over the Arabian Gulf, while minimum values were found over the southern Red Sea and Arabian Sea during the first leg (≤ 0.05 pptv s^{-1}). Maximum P(HCHO) was determined at the center of the Arabian Gulf during the first leg, where elevated mixing ratios of unsaturated hydrocarbons, OVOCs and O$_3$ were observed (Bourtsoukidis et al. 2019, Wang et al. 2020, Tadic et al. 2020). This air mass was characterized by rather low OH mixing ratios, although R(OH) was just slightly elevated (30.07.2017, Fig. 2), which resulted in data points shifted towards the y-axis (Fig. 4). These results also highlight the limits of the method used here, as some reactions yielding HCHO require oxidation of long-lived primary products and are thus temporarily decoupled from measurements of OH and OH reactivity.

In general, compact correlations between P(HCHO) and $[OH] \times R(OH)$ were observed over the Gulf of Aden, the Mediterranean Sea and the Arabian Sea during Leg 1 as indicated by R^2 values between 0.56 and 0.82. Lower R^2 (less than 0.35) were found for the Suez Canal, the Gulf of Oman, the Red Sea South and North, the Arabian Sea during the second leg and the Arabian Gulf. In the area over the Suez Canal the observations indicate a change in chemical composition, as data

5   points are shifted to the left and to the right of the bivariate fit. This area is prominent for its oil and gas exploration as well as high ship traffic, thus it is likely that our results interfere with primary HCHO sources in this region. Wang et al. (2020) also highlight a biomass burning plume in this area, which was excluded from this dataset as it occurred in the early morning and a steady-state analysis is not appropriate. From visual inspection it seems that the low R^2 value over the southern Red Sea is related to the limited span in the P(HCHO) data on the y-axis, while $[OH] \times R(OH)$ covers a broader range of values. The low

10   R^2 for the Arabian Sea during leg 2 results from a cluster of data points at low values on both the x- and the y-axis. In this sub-region there was little variation in chemical composition as air masses (during the Indian summer monsoon) originated from the east coast of Africa (Edtbauer et al., 2020, Tegtmeier et al., 2020). Excluding the contributions of inorganic compounds and other species that yield no HCHO slightly reduced the scatter, but also reduced the overall data coverage (Fig. S1, S2). The results for the Arabian Gulf cover the highest variation of HCHO and VOCs (Bourtsoukidis et al., 2019; Wang et al.,

15   2020) and are characterized by substantial changes in chemical composition. Thus a separation of data (e.g. due to enhanced O_3) would yield different slopes, but we decided not to subdivide the polluted events from the dataset. It is worth mentioning that the Arabian Gulf and the area around the Suez Canal are characterized by potential local sources of HCHO either due to intense ship traffic (Celik et al., 2020) or oil and gas exploration (Bourtsoukidis et al., 2019; Tadic et al., 2020), although obvious point sources with enhanced NO_x, CO, SO_2 mixing ratios were excluded from the entire study. Additional scatter due

20   to wet removal can be excluded for all three regions, due to the absence of rain.

Besides individual data points that do not follow the regression line, the intercept b (P_{add}(HCHO)) of the bivariate fit can be interpreted as a region wide attribution of additional HCHO sources not related to OH chemistry (Eq. 5). The offset b varies between 0.008 pptv s^{-1} over the Arabian Sea during leg 1 and 0.136 pptv s^{-1} in the Arabian Gulf. This enhanced regional contribution of other HCHO sources is most probably due to either direct HCHO emissions or the ozonolysis of alkenes,

25   indicated by elevated levels of O_3 (locally more than 150 ppbv, Tadic et al. 2020) and ethene (Bourtsoukidis et al., 2019), or the photolysis of OVOCs (Wang et al., 2020) and CH_3OOH (Dienhart et al., 2021). The removal of inorganic reactivity and further reactions not leading to HCHO formation (Fig S1, S2) did not change the intercept of the bivariate fits significantly, thus the influence of additional HCHO sources not related to OH chemistry is very likely with the highest values above the Arabian Gulf and the area around Suez Canal.

30   Large variability was observed for the slope m of the regression line for the different regions. As mentioned above, this slope can be equated to the yield α, quantifying the fraction of OH reactivity that results in HCHO production. Inorganic species and CO made up ~ 10 % of the reactivity in most regions and 16 % over the Suez Canal (Pfannerstill et al., 2019) thus the values for α are lower limits when R(OH) is used. Here α varies between 0.014 over the southern Red Sea and 0.258 over the Arabian Gulf, indicating about 1 and 25 % of R(OH) contribution to HCHO production respectively. R(OH)$_{eff}$ was utilized to examine

Atmospheric
Chemistry
and Physics
Discussions

whether α_{eff} would increase drastically compared to α (Fig. 4, S2). By comparing the scatter plots in SU and AS Leg 2 loss of data points is noticeable due to lack of either NO_x, SO_2, CO or O_3 measurements and thus we chose to use both R(OH) and R(OH)$_{eff}$ in this study. The use of R(OH)$_{eff}$ reduced the span on the x-axis significantly, which resulted in increased values for α_{eff} compared to α in five out of the nine sub-regions. The largest increase was determined for the Arabian Gulf (0.315), the

5   Suez Canal (0.115) and the Gulf of Oman (0.077), all of which were rather polluted. The scatter was reduced slightly, being represented by higher R² values. Removal of non-HCHO yielding reactions from total OH reactivity thus indicates that between 1 and 32 % of R(OH)$_{eff}$ contribute to HCHO production. To put these results into perspective, Pfannerstill et al. (2019) compared the R(OH) measurements with the calculated reactivity from all measured species. In general, summation of the measured trace gases resulted in a contribution of unattributed OH reactivity between ~ 20 % over the Arabian Gulf and up to

10 55 % over the Gulf of Aden.

We expect HCHO to be produced from methane (CH_4), non-methane hydrocarbons such as alkanes and alkenes, OVOCs and aromatic hydrocarbons (Wagner et al., 2002). For further analysis, we have recalculated mean reactivities (± 1σ standard deviation) of the individual trace gases (R(OH)$_x$) from alkanes (R(OH)$_{alkanes}$), alkenes (R(OH)$_{alkenes}$), OVOCs without HCHO (R(OH)$_{OVOCS}$) and aromatics (R(OH)$_{aromatics}$) for the different regions (Table 1). Alkanes (including CH_4) contributed on

15 average 3 – 9 %, alkenes 1 – 9 %, OVOCs 8 – 30 % and aromatics 1 – 8 % to the total OH reactivity. Lowest relative contributions of each R(OH)$_x$ to total R(OH) were generally found over the Mediterranean Sea and the Arabian Sea, where also the lowest total OH reactivity has been detected (see Fig. 1 Pfannerstill et al., 2019). Highest relative contributions were observed over the Arabian Gulf, with alkanes and alkenes each contributing ~ 9 % and OVOCs ~ 30 % to the total OH reactivity. The largest relative contribution of aromatic compounds was found over the southern Red Sea (~ 8 %). The sum of

20 alkanes, alkenes, OVOCs and aromatic compounds on average contributed 17 % over the Mediterranean Sea, 27 % over the Suez Canal, 34 % over the southern Red Sea, 27 % over the northern Red Sea, 21 % over the Gulf of Aden, 14 % on the first leg over the Arabian Sea, 32 % over the Gulf of Oman, 55 % over the Arabian Gulf and 21 % on the second leg over the Arabian Sea to the total R(OH).

Table 1: Average ($\pm 1\sigma$ standard deviation) R(OH) for different compound classes (based on the results of Pfannerstill et al., 2019), total R(OH) and α ($\pm$ uncertainty of the slope of the bivariate fit). For NO_x the median values are listed instead of the means.

	R(OH)$_{alkanes}$ s^{-1}	R(OH)$_{alkenes}$ s^{-1}	R(OH)$_{OVOCS}$ s^{-1}	R(OH)$_{aromatics}$ s^{-1}	R(OH) s^{-1}	NO$_x$ ppb$_v$	α
MS	0.323 ± 0.131	0.117 ± 0.179	0.656 ± 0.283	0.105 ± 0.143	7.237 ± 2.928	$0.275 \pm 2,024$	0.045 ± 0.003
SU	0.683 ± 0.546	0.765 ± 1.025	1.118 ± 0.870	0.699 ± 1.178	12.20 ± 5.367	4.806 ± 8.014	0.052 ± 0.008
RS	0.310 ± 0.071	0.781 ± 0.729	1.171 ± 0.444	0.670 ± 0.644	8.715 ± 4.198	0.232 ± 1.208	0.014 ± 0.005
RN	0.449 ± 0.187	0.562 ± 0.522	1.110 ± 0.488	0.386 ± 0.410	9.138 ± 3.316	0.752 ± 5.648	0.026 ± 0.004
GA	0.290 ± 0.039	0.290 ± 0.372	0.861 ± 0.198	0.262 ± 0.344	8.203 ± 3.082	0.604 ± 3.500	0.059 ± 0.006
AS Leg 1	0.270 ± 0.001	0.174 ± 0.073	0.658 ± 0.046	0.114 ± 0.026	8.189 ± 1.896	0.212 ± 0.192	0.019 ± 0.002
GO	0.366 ± 0.100	0.421 ± 0.309	1.504 ± 0.280	0.427 ± 0.334	8.372 ± 3.649	2.596 ± 4.850	0.044 ± 0.007
AG	1.198 ± 1.195	1.208 ± 1.190	3.853 ± 2.438	0.852 ± 0.843	12.92 ± 6.204	1.207 ± 3.997	0.258 ± 0.058
AS Leg 2	0.274 ± 0.016	0.136 ± 0.075	0.476 ± 0.087	0.092 ± 0.061	4.598 ± 0.783	0.155 ± 1.838	0.050 ± 0.003

5   As indicated above, the yield of HCHO from OH × R(OH) is expected to depend on the composition of R(OH) with respect to alkanes, alkenes, OVOCs and aromatic compounds. Mixing ratios of biogenic hydrocarbons, in particular isoprene, were very low with the exception of dimethylsulfide (Edtbauer et al., 2020). All sulfur-containing VOCs together contributed less than 1 % to the total R(OH) and can thus be neglected. In general, the sensitivity of HCHO production to different VOCs results from both the per molecule yield (amount of HCHO produced per VOC molecule lost) and the total emissions of the

10   VOC. As shown by Luecken et al. (2018) for the continental United States, the per-molecule sensitivity for HCHO is highest for anthropogenic emissions of alkenes and comparable within the uncertainties for alkanes, OVOCs and aromatics.

In order to investigate the contribution of different species to HCHO production, Fig. 5 shows scatter plots of α as the lower limit of the HCHO yield versus R(OH)$_{alkanes}$, R(OH)$_{alkenes}$, R(OH)$_{OVOCS}$, and R(OH)$_{aromatics}$, respectively. Bivariate fits indicate linear relationships between α and R(OH)$_{alkanes}$ ($R^2 = 0.83$) and R(OH)$_{OVOCS}$ ($R^2 = 0.89$), while less linear relationships are

15   obtained for R(OH)$_{alkenes}$ ($R^2 = 0.48$) and R(OH)$_{aromatics}$ ($R^2 = 0.34$). The results of these scatter plots are determined by the measurements over the Arabian Gulf and that the AQABA dataset did not have sufficient coverage of moderately polluted conditions. The span (maximum – minimum in Table 1) in R(OH)$_x$ is highest for the OVOCs (3.3 s^{-1}), while alkanes and alkenes are comparable (~ 1 s^{-1}). The range for aromatics is smaller at 0.6 s^{-1}. Since the span in α (maximum – minimum in Table 1) is the same for all plots, the slopes are a measure of the increase in α for an increase of R(OH)$_x$ by 1 s^{-1}. This slope is

20   comparable (within its uncertainties) for alkanes (0.227 $\pm$ 0.039 s^{-1}), aromatics (0.162 $\pm$ 0.081 s^{-1}) and alkenes (0.143 $\pm$ 0.056 s^{-1}), while it is approximately a factor of two lower for the HCHO yield from OVOCs (0.070 $\pm$ 0.009 s^{-1}).
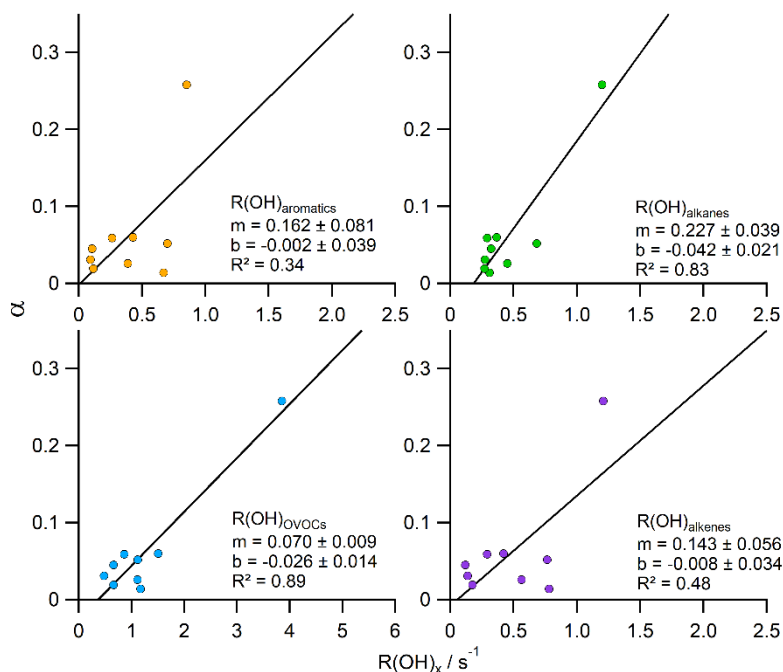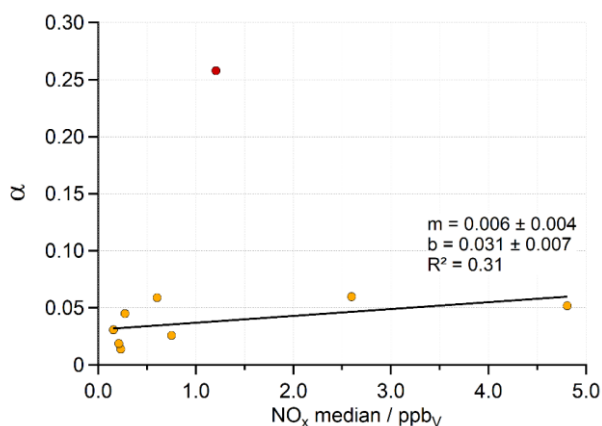
Figure 5: Scatter plot of the HCHO yield α (calculated with R(OH) via Eq. 1) as a function of the separated OH reactivity ($R(OH)_x$) towards different VOC families (aromatics, alkanes, alkenes, and oxidized volatile organic compounds).

Bivariate fits were also performed without the contribution of inorganics, CO and HCHO ($R(OH)_{eff}$), which increased the slopes and showed a slightly more distinct correlation with overall similar results (Fig. S3). These results indicate that the immediate HCHO yield α increases linearly with an increase in OH reactivity towards alkanes and OVOCs. Also, an absolute increase in $R(OH)_x$ is mostly accompanied by an increase of α, although there is no clear correlation towards $R(OH)_{aromatics}$ and $R(OH)_{alkenes}$. Our results are not directly comparable to the ordering by Luecken et al. (2018), since in their analysis reactions with O_3 (alkenes) and photolysis of HCHO precursors (OVOCs) were included. These sources of HCHO are not represented by $R(OH)_x$ used in our study.

The yield of HCHO can also be a function of NO_x levels if there are processes (at low NO) that lead to formation of e.g. peroxides rather than HCHO (Wolfe et al., 2016). Figure 6 shows the relationship between α for the different regions and corresponding median NO_x levels (Table 1). We used median NO_x levels instead of means to limit the impact of plumes from passing ships and other point sources (Celik et al., 2020), although our conclusions do not change for mean values. Figure 6 shows that α and NO_x are not well correlated. Only if the data points with the highest median NO_x mixing ratios, measured in Suez Canal (4.8 ppbv) and the Gulf of Oman (2.6 ppbv), or the single data point representing the Arabian Gulf (red data point in Fig. 6), are removed from the bivariate fits, significant correlations are obtained. Indeed, the role of NO_x in HCHO production is ambiguous. On the one hand, the yield of HCHO from peroxy radicals is expected to be NO_x dependent (at NO_x

≤ 100 pptv the reaction of peroxy radicals with HO_2 (to form hydroperoxides) will reduce the yield of HCHO), but NO also influences the amount of OH radicals available e.g. due to recycling of HO_2 (Valin et al., 2016).

Figure 6: Scatter plot of the HCHO yield α (deduced from the slopes m in Figure 4) versus median NO_x mixing ratios. The outlier for the Arabian Gulf (red point) has been discarded for the York-Fit.

This result is in accord with the fact that very clean background MBL air was rarely sampled during AQABA (lowest median NO_x of 0.16 ppbv over AS Leg 2). Tadic et al. (2020) also showed that most regions were in the O_3 production regime (signaling sufficient NO) and thus also the production of HCHO was not NO_x limited. Based on this rather polluted data set, we cannot identify under which NO_x conditions a potential enhancement of α could occur. Luecken et al. (2018) used a photochemical air quality model to identify the sensitivity of HCHO concentrations across the United States to hydrocarbon speciation and NO_x. They found that HCHO production is similar under low and high-NO_x chemistry, indicating that HCHO concentrations are less sensitive to NO_x as e.g. the formation of O_3.

5 Summary and conclusions

In-situ observations of HCHO and its sinks due to reaction with OH, photolysis and dry deposition to the ocean surface have been compared to its production from the reaction of OH with VOCs by using the total OH reactivity (R(OH)) and measured

5   OH concentrations during the AQABA ship campaign around the Arabian Peninsula. Large variation of HCHO mixing ratios about more than an order of magnitude with maximum values (up to ~ 12 ppbv) in the center of the Arabian Gulf highlighted the region as a hotspot of photochemical air pollution ($\geq$ 150 ppbv O_3, Tadic et al., 2020). Lowest concentrations of HCHO and its precursors identified the Arabian Sea as the cleanest region of the measurement campaign, related to the stable winds of the Indian summer monsoon, originating near the east coast of Africa (Edtbauer et al., 2020). Surprisingly clean air was

10 also detected in the southern Red Sea. In photo-stationary state, compact relationships between HCHO production and loss were found for some regions along the ship track. The yield of HCHO from reactions of OH differs from region to region and depends largely on the presence of VOCs, with lowest values (less than 2 %) deduced over the Arabian Sea during the first leg and the southern Red Sea, and highest values (~ 32 %) over the Arabian Gulf. In most regions less than 6 % of total OH reactivity contributed to HCHO production and up to 16 % was due to reactions with inorganic trace-gases. Excluding

15 inorganic reactivity and non-HCHO yielding reactions from total R(OH) slightly improved the correlation between production and loss of HCHO, although the calculated yield α just increased moderately. In general, the yield of HCHO increased with the absolute contributions from alkanes, alkenes, OVOCs and aromatics to R(OH). A clear dependence of α on NO_x could not be identified, which is likely related to shortage of very clean (i.e. low NO_x) conditions during the AQABA campaign.

20 *Data availability*. All AQABA data sets used in this study are permanently stored in an archive on the KEEPER service of the Max Planck Digital Library (https://keeper.mpdl.mpg.de; last access: 9 February 2021) and are available to all scientists, which agree to the AQABA data protocol.

Competing interests. The authors declare that they have no conflict of interest.

25

Author contributions. HF and DD designed the study. DD and BH performed the HCHO measurements. IT and UP provided the NO_x measurements. RR, ST, MM and HH performed the LIF OH and HO_2 measurements during AQABA. EP and NW provided the OH reactivity measurements. NW, AE and CS were responsible and OVOC measurements. EB and LE carried out the VOC measurements during AQABA, which were used together with the OVOCs by EP to calculate speciated OH

30 reactivity. JW supervised the VOC, OVOC and OH reactivity measurements. PE and JNC performed the O_3 and SO_2 measurements during AQABA. JS and JNC provided the actinic flux measurements and calculated photolysis rates. JL designed and supervised the AQABA project.

Atmospheric
Chemistry
and Physics
Discussions

Atmospheric
Chemistry
and Physics
Discussions

References

Anderson, D. C., Nicely, J. M., Wolfe, G. M., Hanisco, T. F., Salawitch, R. J., Canty, T. P., Dickerson, R. R., Apel, E. C., Baidar, S., Bannan, T. J., Blake, N. J., Chen, D., Dix, B., Fernandez, R. P., Hall, S. R., Hornbrook R. S., Huey, L. G., Josse, B., Jöckel, P., Kinnision, D. E., Koenig, T. K., Le Breton, M., Marécal, V., Morgenstern, O., Oman, L. D., Pan, L. L., Percival, C., Plummer, D., Revell, L. E., Rozanow, E., Saiz-Lopez, A., Stenke, A., Sudo, K., Tilmes S., Ullmann, K., Volkamer, R., Weinheimer, A. J. and Zeng, G.: Formaldehyde in the tropical western Pacific: Chemical sources and sinks, convective transport, and representation in CAM-Chem and the CCMI models. Journal of Geophysical Research: Atmospheres, 122, 11, 201– 11, 226, https://doi.org/10.1002/2016JD026121, 2017.

Ayers, G.P., Gillet, R.W., Granek, H., de Sreves, C., and Cox, R.A.: Formaldehyde production in clean marine air, Geophys. Res. Lett., 24, 401-404, https://doi.org/10.1029/97GL00123, 1997.

Bourtsoukidis, E., Ernle, L., Crowley, J. N., Lelieveld, J., Paris, J.-D., Pozzer, A., Walter, D., and Williams, J.: Non-methane hydrocarbon (C_2–C_8) sources and sinks around the Arabian Peninsula, Atmos. Chem. Phys., 19, 7209–7232, https://doi.org/10.5194/acp-19-7209-2019, 2019.

Celik, S., Drewnick, F., Fachinger, F., Brooks, J., Darbyshire, E., Coe, H., Paris, J.-D., Eger, P. G., Schuladen, J., Tadic, I., Friedrich, N., Dienhart, D., Hottmann, B., Fischer, H., Crowley, J. N., Harder, H., and Borrmann, S.: Influence of vessel characteristics and atmospheric processes on the gas and particle phase of ship emission plumes: in situ measurements in the Mediterranean Sea and around the Arabian Peninsula, Atmos. Chem. Phys., 20, 4713–4734, https://doi.org/10.5194/acp-20-4713-2020, 2020.

Cox, R. A., Ammann, M., Crowley, J. N., Herrmann, H., Jenkin, M. E., McNeill, V. F., Mellouki, A., Troe, J., and Wallington, T. J.: Evaluated kinetic and photochemical data for atmospheric chemistry: Volume VII – Criegee intermediates, Atmos. Chem. Phys., 20, 13497–13519, https://doi.org/10.5194/acp-20-13497-2020, 2020.

De Smedt, I., Müller, J.-F., Stavrakou, T., van der A, R., Eskes, H., and Van Roozendael, M.: Twelve years of global observations of formaldehyde in the troposphere using GOME and SCIAMACHY sensors, Atmos. Chem. Phys., 8, 4947– 4963, https://doi.org/10.5194/acp-8-4947-2008, 2008.

De Smedt, I., Van Roozendael, M., Stavrakou, T., Müller, J.-F., Lerot, C., Theys, N., Valks, P., Hao, N., and van der A, R.: Improved retrieval of global tropospheric formaldehyde columns from GOME-2/MetOp-A addressing noise reduction and instrumental degradation issues, Atmos. Meas. Tech., 5, 2933–2949, https://doi.org/10.5194/amt-5-2933-2012, 2012.

De Smedt, I., Stavrakou, T., Hendrick, F., Danckaert, T., Vlemmix, T., Pinardi, G., Theys, N., Lerot, C., Gielen, C., Vigouroux, C., Hermans, C., Fayt, C., Veefkind, P., Müller, J.-F., and Van Roozendael, M.: Diurnal, seasonal and long-term variations of

global formaldehyde columns inferred from combined OMI and GOME-2 observations, Atmos. Chem. Phys., 15, 12519–12545, https://doi.org/10.5194/acp-15-12519-2015, 2015.

De Smedt, I., Theys, N., Yu, H., Danckaert, T., Lerot, C., Compernolle, S., Van Roozendael, M., Richter, A., Hilboll, A., Peters, E., Pedergnana, M., Loyola, D., Beirle, S., Wagner, T., Eskes, H., van Geffen, J., Boersma, K. F., and Veefkind, P.:
5   Algorithm theoretical baseline for formaldehyde retrievals from S5P TROPOMI and from the QA4ECV project, Atmos. Meas. Tech., 11, 2395–2426, https://doi.org/10.5194/amt-11-2395-2018, 2018.

DiGangi, J. P., Henry, S. B., Kammrath, A., Boyle, E. S., Kaser, L., Schnitzhofer, R., Graus, M., Turnipseed, A., Park, J.-H., Weber, R. J., Hornbrook, R. S., Cantrell, C. A., Maudlin III, R. L., Kim, S., Nakashima, Y., Wolfe, G. M., Kajii, Y., Apel, E. C., Goldstein, A. H., Guenther, A., Karl, T., Hansel, A., and Keutsch, F. N.: Observations of glyoxal and formaldehyde as
10   metrics for the anthropogenic impact on rural photochemistry, Atmos. Chem. Phys., 12, 9529–9543, https://doi.org/10.5194/acp-12-9529-2012, 2012.

Dienhart, D., Hottmann, B., Crowley, J. N., Eger, P. G., Hafermann, S., Harder, H., Röder, L., Martinez, M., Parchatka, U., Pozzer, A., Rohloff, R., Schuladen, J., Tadic, I., Tauer, S., Walter, D., Lelieveld, J., Fischer, H.: Formaldehyde (HCHO) and Hydroperoxide distribution around the Arabian Peninsula – A comparison of ship-based measurements with the general
15   circulation model EMAC, Atmos. Chem. Phys., in preparation.

Duncan, B. N., Yoshida, Y., Olson, J. R., Sillman, S., Martin, R. V., Lamsal, L., Hu, Y., Pickering, K. E., Retscher, C., Allen, D. J., Crawford, J. H.: Application of OMI observations to a space-based indicator of NO$_x$ and VOC controls on surface ozone formation, J. Atmos. Env., 44, 2213-2223, https://doi.org/10.1016/j.atmosenv.2010.03.010, 2010.

Edtbauer, A., Stönner, C., Pfannerstill, E. Y., Berasategui, M., Walter, D., Crowley, J. N., Lelieveld, J., and Williams, J.: A
20   new marine biogenic emission: methane sulfonamide (MSAM), dimethyl sulfide (DMS), and dimethyl sulfone (DMSO$_2$) measured in air over the Arabian Sea, Atmos. Chem. Phys., 20, 6081–6094, https://doi.org/10.5194/acp-20-6081-2020, 2020.

Eger, P. G., Friedrich, N., Schuladen, J., Shenolikar, J., Fischer, H., Tadic, I., Harder, H., Martinez, M., Rohloff, R., Tauer, S., Drewnick, F., Fachinger, F., Brooks, J., Darbyshire, E., Sciare, J., Pikridas, M., Lelieveld, J., and Crowley, J. N.: Shipborne measurements of ClNO$_2$ in the Mediterranean Sea and around the Arabian Peninsula during summer, Atmos. Chem. Phys., 19,
25   12121–12140, https://doi.org/10.5194/acp-19-12121-2019, 2019.

Fried, A., Cantrell, C., Olson, J., Crawford, J. H., Weibring, P., Walega, J., Richter, D., Junkermann, W., Volkamer, R., Sinreich, R., Heikes, B. G., O'Sullivan, D., Blake, D. R., Blake, N., Meinardi, S., Apel, E., Weinheimer, A., Knapp, D., Perring, A., Cohen, R. C., Fuelberg, H., Shetter, R. E., Hall, S. R., Ullmann, K., Brune, W. H., Mao, J., Ren, X., Huey, L. G., Singh, H. B., Hair, J. W., Riemer, D., Diskin, G., and Sachse, G.: Detailed comparisons of airborne formaldehyde measurements with
30   box models during the 2006 INTEX-B and MILAGRO campaigns: potential evidence for significant impacts of unmeasured

and multi-generation volatile organic carbon compounds, Atmos. Chem. Phys., 11, 11867–11894, https://doi.org/10.5194/acp-11-11867-2011, 2011.

Friedrich, N., Eger, P., Shenolikar, J., Sobanski, N., Schuladen, J., Dienhart, D., Hottmann, B., Tadic, I., Fischer, H., Martinez, M., Rohloff, R., Tauer, S., Harder, H., Pfannerstill, E. Y., Wang, N., Williams, J., Brooks, J., Drewnick, F., Su, H., Li, G., Cheng, Y., Lielieveld, J., and Crowley, J. N.: Reactive nitrogen around the Arabian Peninsula and in the Mediterranean Sea during the 2017 AQABA ship campaign, Atmos. Chem. Phys. Discuss. [preprint], https://doi.org/10.5194/acp-2021-42, in review, 2021.

Fuchs, H., Novelli, A., Rolletter, M., Hofzumahaus, A., Pfannerstill, E. Y., Kessel, S., Edtbauer, A., Williams, J., Michoud, V., Dusanter, S., Locoge, N., Zannoni, N., Gros, V., Truong, F., Sarda-Esteve, R., Cryer, D. R., Brumby, C. A., Whalley, L. K., Stone, D., Seakins, P. W., Heard, D. E., Schoemaecker, C., Blocquet, M., Coudert, S., Batut, S., Fittschen, C., Thames, A. B., Brune, W. H., Ernest, C., Harder, H., Muller, J. B. A., Elste, T., Kubistin, D., Andres, S., Bohn, B., Hohaus, T., Holland, F., Li, X., Rohrer, F., Kiendler-Scharr, A., Tillmann, R., Wegener, R., Yu, Z., Zou, Q., and Wahner, A.: Comparison of OH reactivity measurements in the atmospheric simulation chamber SAPHIR, Atmos. Meas. Tech., 10, 4023–4053, https://doi.org/10.5194/amt-10-4023-2017, 2017.

Hens, K., Novelli, A., Martinez, M., Auld, J., Axinte, R., Bohn, B., Fischer, H., Keronen, P., Kubistin, D., Nölscher, A. C., Oswald, R., Paasonen, P., Petäjä, T., Regelin, E., Sander, R., Sinha, V., Sipilä, M., Taraborrelli, D., Tatum Ernest, C., Williams, J., Lielieveld, J., and Harder, H.: Observation and modelling of HOx radicals in a boreal forest, Atmos. Chem. Phys., 14, 8723-8747, https://doi.org/10.5194/acp-14-8723-2014, 2014.

Klippel, T., Fischer, H., Bozem, H., Lawrence, M. G., Butler, T., Jöckel, P., Tost, H., Martinez, M., Harder, H., Regelin, E., Sander, R., Schiller, C. L., Stickler, A., and Lielieveld, J.: Distribution of hydrogen peroxide and formaldehyde over Central Europe during the HOOVER project, Atmos. Chem. Phys., 11, 4391–4410, https://doi.org/10.5194/acp-11-4391-2011, 2011.

Kluge, F., Hüneke, T., Knecht, M., Lichtenstern, M., Rotermund, M., Schlager, H., Schreiner, B., and Pfeilsticker, K.: Profiling of formaldehyde, glyoxal, methylglyoxal, and CO over the Amazon: normalized excess mixing ratios and related emission factors in biomass burning plumes, Atmos. Chem. Phys., 20, 12363–12389, https://doi.org/10.5194/acp-20-12363-2020, 2020.

Kormann, R., Fischer, H., de Reus, M., Lawrence, M., Brühl, Ch., von Kuhlmann, R., Holzinger, R., Williams, J., Lielieveld, J., Warneke, C., de Gouw, J., Heland, J., Ziereis, H., and Schlager, H.: Formaldehyde over the eastern Mediterranean during MINOS: Comparison of airborne in-situ measurements with 3D-model results, Atmos. Chem. Phys., 3, 851–861, https://doi.org/10.5194/acp-3-851-2003, 2003.

Liebmann, J. M., Muller, J. B. A., Kubistin, D., Claude, A., Holla, R., Plass-Dülmer, C., Lielieveld, J., and Crowley, J. N.: Direct measurements of NO3 reactivity in and above the boundary layer of a mountaintop site: identification of reactive trace

Atmospheric
Chemistry
and Physics
Discussions

gases and comparison with OH reactivity, Atmos. Chem. Phys., 18, 12045–12059, https://doi.org/10.5194/acp-18-12045-2018, 2018.

Liu, L., Flatøy, F., Ordóñez, C., Braathen, G. O., Hak, C., Junkermann, W., Andreani-Aksoyoglu, S., Mellqvist, J., Galle, B., Prévôt, A. S. H., and Isaksen, I. S. A.: Photochemical modelling in the Po basin with focus on formaldehyde and ozone, Atmos. Chem. Phys., 7, 121–137, https://doi.org/10.5194/acp-7-121-2007, 2007.

Luecken, D. J., Napelenok, S. L., Strum, M., Scheffe, R., and Phillips, S.: Sensitivity of ambient atmospheric formaldehyde and ozone to precursor species and source types across the United States, Environ. Sci. Technol., 52, 4668-4675, https://doi.org/10.1021/acs.est.7b05509, 2018.

Marbach, T., Beirle, S., Platt, U., Hoor, P., Wittrock, F., Richter, A., Vrekoussis, M., Grzegorski, M., Burrows, J. P., and Wagner, T.: Satellite measurements of formaldehyde linked to shipping emissions, Atmos. Chem. Phys., 9, 8223–8234, https://doi.org/10.5194/acp-9-8223-2009, 2009.

Martin, R. V., Fiore, A. M., and Van Donkelaar, A.: Space-based diagnosis of surface ozone sensitivity to anthropogenic emissions, Geophys. Res. Lett., 31, L06120, doi:10.1029/2004GL019416, 2004.

Martinez, M., Harder, H., Kubistin, D., Rudolf, M., Bozem, H., Eerdekens, G., Fischer, H., Klüpfel, T., Gurk, C., Königstedt, R., Parchatka, U., Schiller, C. L., Stickler, A., Williams, J., and Lelieveld, J.: Hydroxyl radicals in the tropical troposphere over the Suriname rainforest: airborne measurements, Atmos. Chem. Phys., 10, 3759-3773, https://doi.org/10.5194/acp-10-3759-2010, 2010.

Millet, D. B., Jacob, D. J., Boersma, K. F., Fu, T. M., Kurosu, T. P., Chance, K., Heald, C. L., and Guenther, A.: Spatial distribution of isoprene emissions from North America derived from formaldehyde column measurements by the OMI satellite sensor, J. Geophys. Res., 113, D02307, https://doi10.1029/2007JD008950, 2008.

Novelli, A., Hens, K., Tatum Ernest, C., Kubistin, D., Regelin, E., Elste, T., Plass-Dülmer, C., Martinez, M., Lelieveld, J., and Harder, H.: Characterisation of an inlet pre-injector laser-induced fluorescence instrument for the measurement of atmospheric hydroxyl radicals, Atmos. Meas. Tech., 7, 3413-3430, https://doi.org/10.5194/amt-7-3413-2014, 2014.

Palmer, P. I., Jacob, D. J., Fiore, A. M., Martin, R. V., Chance, K., and Kurosu, T. P.: Mapping isoprene emissions over North America using formaldehyde column observations from space, J. Geophys. Res., 108, 4180, doi:10.1029/2002JD002153, 2003.

Pfannerstill, E. Y., Wang, N., Edtbauer, A., Bourtsoukidis, E., Crowley, J. N., Dienhart, D., Eger, P. G., Ernle, L., Fischer, H., Hottmann, B., Paris, J.-D., Stönner, C., Tadic, I., Walter, D., Lelieveld, J., and Williams, J.: Shipborne measurements of total OH reactivity around the Arabian Peninsula and its role in ozone chemistry, Atmos. Chem. Phys., 19, 11501–11523, https://doi.org/10.5194/acp-19-11501-2019, 2019.

Parrish, D. D., Ryerson, T. B., Mellqvist, J., Johansson, J., Fried, A., Richter, D., Walega, J. G., Washenfelder, R. A., de Gouw, J. A., Peischl, J., Aikin, K. C., McKeen, S. A., Frost, G. J., Fehsenfeld, F. C., and Herndon, S. C.: Primary and secondary sources of formaldehyde in urban atmospheres: Houston Texas region, Atmos. Chem. Phys., 12, 3273–3288, https://doi.org/10.5194/acp-12-3273-2012, 2012.

5   Paris, J.-D., Riandet, A., Bourtsoukidis, E., Delmotte, M., Berchet, A., Williams, J., Ernle, L., Tadic, I., Harder, H., and Lelieveld, J.: Shipborne measurements of methane and carbon dioxide in the Middle East and Mediterranean areas and contribution from oil and gas emissions, Atmos. Chem. Phys. Discuss. [preprint], https://doi.org/10.5194/acp-2021-114, in review, 2021.

Reeves, C. E. and Penkett, S. A.: Measurements of peroxides and what they tell us, Chem. Rev., 103, 12, 5199–5218,
10   doi:10.1021/cr0205053, 2003.

Schroeder, J. R., Crawford, J. H., Fried, A., Walega, J., Weinheimer, A., Wisthaler, A., Müller, M., Mikoviny, T., Chen, G., Shook, M., Blake, D. R., Tonnesen, G. S.: New insights into the column CH_2O/NO_2 ratio as an indicator of near-surface ozone sensitivity, J. Geophys. Res. Atmos., 122, 8885–8907, doi:10.1002/2017JD026781, 2017.

Shim, C., Wang, Y., Choi, Y., Palmer, P. I., Abbot, D. S., and Chance, K.: Constraining global isoprene emissions with Global
15   Ozone Monitoring Experiment (GOME) formaldehyde column measurements, J. Geophys. Res., 110, D24301, https://doi.org/10.1029/2004JD005629, 2005.
Sinha, V., Williams, J., Crowley, J. N., and Lelieveld, J.: The Comparative Reactivity Method – a new tool to measure total OH Reactivity in ambient air, Atmos. Chem. Phys., 8, 2213–2227, https://doi.org/10.5194/acp-8-2213-2008, 2008.

Stickler, A., Fischer, H., Williams, J., de Reus, M., Sander, R., Lawrence, M. G., Crowley, J. N., and Lelieveld, J.: Influence
20   of summertime deep convection on formaldehyde in the middle and upper troposphere over Europe, J. Geophys. Res., 111, D14308, doi:10.1029/2005JD007001, 2006.

Stickler, A., Fischer, H., Bozem, H., Gurk, C., Schiller, C., Martinez-Harder, M., Kubistin, D., Harder, H., Williams, J., Eerdekens, G., Yassaa, N., Ganzeveld, L., Sander, R., and Lelieveld, J.: Chemistry, transport and dry deposition of trace gases in the boundary layer over the tropical Atlantic Ocean and the Guyanas during the GABRIEL field campaign, Atmos. Chem.
25   Phys., 7, 3933–3956, https://doi.org/10.5194/acp-7-3933-2007, 2007.

Tadic, I., Crowley, J. N., Dienhart, D., Eger, P., Harder, H., Hottmann, B., Martinez, M., Parchatka, U., Paris, J.-D., Pozzer, A., Rohloff, R., Schuladen, J., Shenolikar, J., Tauer, S., Lelieveld, J., and Fischer, H.: Net ozone production and its relationship to nitrogen oxides and volatile organic compounds in the marine boundary layer around the Arabian Peninsula, Atmos. Chem. Phys., 20, 6769–6787, https://doi.org/10.5194/acp-20-6769-2020, 2020.

Tegtmeier, S., Marandino, C., Jia, Y., Quack, B., and Mahajan, A. S.: Atmospheric gas-phase composition over the Indian Ocean, Atmos. Chem. Phys. Discuss. [preprint], https://doi.org/10.5194/acp-2020-718, in review, 2020.

Valin, L. C., Fiore, A. M., Chance, K., and González Abad, G.: The role of OH production in interpreting the variability of CH_2O columns in the southeast U.S., J. Geophys. Res. Atmos., 121, 478– 493, doi:10.1002/2015JD024012, 2016.

5   Wagner, V., von Glasow, R., Fischer, H., and Crutzen, P. J., Are CH_2O measurements in the marine boundary layer suitable for testing the current understanding of CH_4 photooxidation? : A model study, J. Geophys. Res., 107 (D3), doi:10.1029/2001JD000722, 2002.

Wang, N., Edtbauer, A., Stönner, C., Pozzer, A., Bourtsoukidis, E., Ernle, L., Dienhart, D., Hottmann, B., Fischer, H., Schuladen, J., Crowley, J. N., Paris, J.-D., Lelieveld, J., and Williams, J.: Measurements of carbonyl compounds around the
10   Arabian Peninsula: overview and model comparison, Atmos. Chem. Phys., 20, 10807–10829, https://doi.org/10.5194/acp-20-10807-2020, 2020.

Weller, R., Schrems, O., Boddenberg, A., Gäb, S., and Gautrois, M.: Meridional distribution of hydroperoxides and formaldehyde in the marine boundary layer of the Atlantic (48°N-35°S) measured during the Albatross campaign, J. Geophys. Res., 105 (D11), 14401– 14412, doi:10.1029/1999JD901145, 2000.

15   Wennberg, P. O., Bates, K. H., Crounse, J. D., Dodson, L. G., Mc-Vay, R. C., Mertens, L. A., Nguyen, T. B., Praske, E., Schwantes, R. H., Smarte, M. D., St Clair, J. M., Teng, A. P., Zhang, X., and Seinfeld, J. H.: Gas-Phase Reactions of Isoprene and Its Major Oxidation Products, Chem. Rev., 118, 3337–3390, https://doi.org/10.1021/acs.chemrev.7b00439, 2018.
Williams, J. and Brune, W.: A roadmap for OH reactivity research, Atmos. Environ., 106, 371–372, https://doi.org/10.1016/j.atmosenv.2015.02.017, 2015.
20   Wolfe, G. M., Kaiser, J., Hanisco, T. F., Keutsch, F. N., de Gouw, J. A., Gilman, J. B., Graus, M., Hatch, C. D., Holloway, J., Horowitz, L. W., Lee, B. H., Lerner, B. M., Lopez-Hilifiker, F., Mao, J., Marvin, M. R., Peischl, J., Pollack, I. B., Roberts, J. M., Ryerson, T. B., Thornton, J. A., Veres, P. R., and Warneke, C.: Formaldehyde production from isoprene oxidation across NO_x regimes, Atmos. Chem. Phys., 16, 2597–2610, https://doi.org/10.5194/acp-16-2597-2016, 2016.
Wolfe, G.M., Nicely, J.M., St. Clair, J.M., Hanisco, T.F., Liao, J., Oman, L.D., Brune, W.B., Miller, D., Thames, A., Gonzalez
25   Abad, G., Ryerson, T.B., Thompson, C.R., Peischl, J., McCain, K., Sweeney, C., Wennberg, P.O., Kim, M., Crounse, J.D., Hall, S.R., Ullmann, K., Diskin, G., Bui, P., Chang, C., and Dean-Day, J.: Mapping hydroxyl variability throughout the global remote troposphere via synthesis of airborne and satellite formaldehyde observations. PNAS, 116, 11171-11180, https://doi.org/10.1073/pnas.1821661116, 2019.

York, D., Evensen, N.M., Lopez Martinez, M., and De Basabe Delgado, J.: Unified equations for the slope, intercept, and
30   standard errors of the best straight line, Am. J. Phys., 72, 367-375, https://doi.org/10.1119/1.1632486, 2004.

Zhu, L., González Abad, G., Nowlan, C. R., Chan Miller, C., Chance, K., Apel, E. C., DiGangi, J. P., Fried, A., Hanisco, T. F., Hornbrook, R. S., Hu, L., Kaiser, J., Keutsch, F. N., Permar, W., St. Clair, J. M., and Wolfe, G. M.: Validation of satellite formaldehyde (HCHO) retrievals using observations from 12 aircraft campaigns, Atmos. Chem. Phys., 20, 12329–12345, https://doi.org/10.5194/acp-20-12329-2020, 2020.